International Journal of Research in Engineering and Science (IJRES)
ISSN (Online): 2320-9364, ISSN (Print): 2320-9356
www.ijres.org Volume 4 Issue 7 ǁ Jul. 2016 ǁ PP.97-108

Comparative study for ball, conic and GRIN rod lens coupling schemes using Zemax Huygen's physical optics calculations

Nikhilesh Kumar, Prakash Kumar Behera, Subrat Kumar Panda, Sulochana Nanda

Department of Electronics and Communication Engineering, NM Institute of Engineering and Technology,Bhubaneswar , Odisha
Department of Electronics and Communication Engineering, Raajdhani Engineering College,Bhubaneswar,Odisha
Department of Electronics and Communication Engineering,Aryan Institute of Engineering and Technology Bhubnaeswar , Odisha
Department of Electronics and Communication Engineering,Capital Engineering College,Bhubaneswar,Odisha

ABSTRACT: *In this work, numerical coupling efficiency calculations comparing single-mode fiber (SMF) to SMF cou-pling schemes using uncoated single ball, conic and graded-index (GRIN) rod lenses are discussed. The reported fiber coupling efficiency (FCE) calculations were performed using Huygens integral and Gaussian beam physical optics propagation (GBPOP) features in Zemax® . The Huygens integral method results indicate that the FCE for ball, conic and GRIN rod single uncoated lenses (without accounting for Fresnel reflection and bulk absorption effects) can reach with the optimal lens and fiber parameters 91.11% (N-BK7 glass), 99.68% (N-BK7 glass) and 96.58%, respectively. In comparison, the calculated FCE for uncoated N-BK7 glass ball lens using the GBPOP method was 87.22% (without accounting for Fresnel reflections and bulk absorption effects). Furthermore, FCE calculations for ball lenses made out of sapphire, fused silica, S-LAH79 and N-LASF9 glass are given. The calculated deviation between the GBPOP and Huygens integral methods is <0.5%. Finally, tolerance analysis for each lens coupling scheme relating FCE to the tilts and the decentering of the lens and the two fibers is provided. The tolerance analysis calculations indicate that decentering of fibers and the single lens has the highest impact on the FCE values. Finally, FCE results suggest that the GRIN lens coupling scheme is the most sensitive scheme to misalignment and the ball lens scheme is the least sensitive to misalignment.*

Keywords:
Fiber coupling efficiency (FCE)
Gaussian beam physical optics propagation (GBPOP) method
Huygens integral method
Single-mode fiber (SMF)
Tolerance analysis

I. INTRODUCTION

Efficient coupling into single-mode or multimode optical fibers [1] is essential for many fiber-optic laser beam delivery applica-tions such as telecommunications, oil and gas fiber-optic sensors, laser angioplasty, biomedical fiber-optic cables, multi-cell laser excitation systems, turbine engines fluorescence thermometry and static pressure measurements, endoscopy, fiber amplifiers, and fiber lasers [2–7].

In order to couple a laser beam efficiently into the core of SMF a lens is used for focusing and shaping the laser beam into a spot size less than 10 m in diameter. Ball [8–10], conic [11–13] and GRIN rod [14,15] lenses offer several advantages for coupling laser beams into SMFs because of their low cost, small size, ease of packaging and ease of alignment. Fiber coupling efficiency (FCE) [16–18] is defined as the fraction of the laser power emitted from the light source and coupled into the receiving fiber and can be impacted by Fresnel reflection losses, lens aberrations, surface quality of the fiber endface and the misalignment of the system components.

The purpose of this work is to present FCE calculations between SMF-to-SMF using uncoated single ball, conic and GRIN rod lens couplings schemes. The FCE calculations were performed using Huygens integral and the Gaussian beam physical optics propaga-tion (GBPOP) methods [19] in Zemax [20–23]. Moreover, tolerance analysis relating FCE [24] to the lens, source fiber and receive fiber tilts and decentering is provided.

II. BALL, CONIC AND GRIN ROD LENS SM FIBER-TO-SM FIBER COUPLING SCHEMES

The ball, conic and GRIN rod single lens SMF-to-SMF [25] cou-pling schemes are schematically shown in Figs. 1–3.

All FCE calculations performed in this article were for uncoated ball, conic and GRIN rod single lenses. The FCE calculations were carried out without accounting for Fresnel reflections and bulk material absorption effects. However, an estimate for the con-tribution of Fresnel reflections and bulk material absorption is provided. In addition, all FCE calculations were performed by set-ting the numerical aperture (NA) for the source and the receiving fiber to 0.09 (Corning defines the NA at 1% of the peak center [25]) and the Gaussian input beam radial waist to 4.6 m (the mode field diameter at 1310 nm = 9.2 $\pm$ 0.4 m [25]). Further, the FCE for each lens scheme was maximized (optimized) by adjust-ing the separation (thickness) between the lens-to-source fiber and lens-to-receiving fiber using the FICL operand in Zemax. The FCE were performed at 1310 nm due to the availability of MFD val-ues at this wavelength. For the Huygens integral method 128 × 128 (x-sampling × y-sampling) was selected to perform the FCE numer-ical calculations and 1024 × 1024 (x-sampling × y-sampling) for the GBPOP method. The selection of the x and y sampling values was chosen by increasing the x and y sampling until no changes was observed in the calculated FCE value. Increasing the sampling can result in a significant increase in the computation time for both methods. Here, it is worth noting that calculations performed using the Huygens integral method is slower than the GBPOP method and can take few minutes for large x and y sampling values.

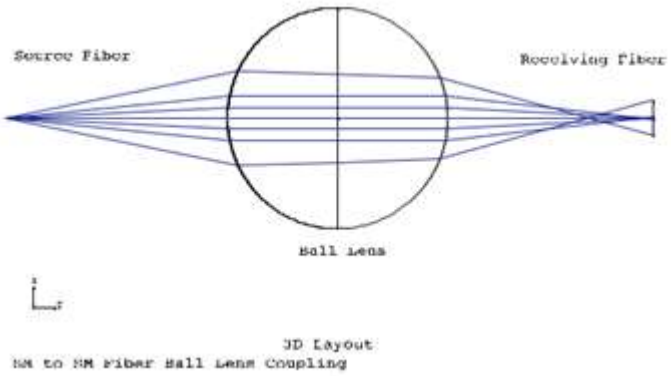

Fig. 1. Diagram depicting the SMF-to-SMF coupling using uncoated ball lens (lens diameter = 2.00 mm, source fiber-lens separation = 2.012 mm, receiving fiber-lens separation = 1.863 mm, total track = 5.875 mm).

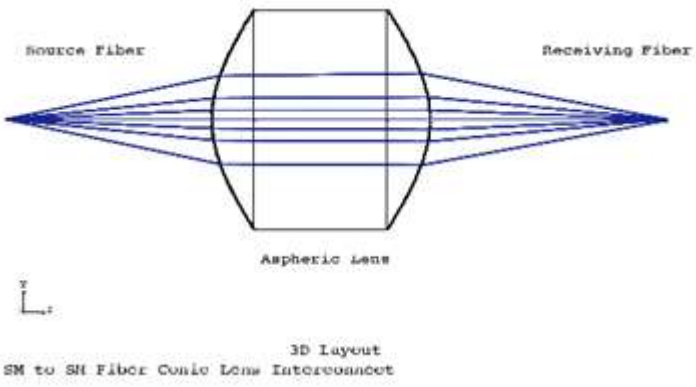

Fig. 2. Diagram showing the SMF-to-SMF coupling using uncoated aspheric lens (Lens diameter = 2.00 mm; Lens length = 2.000 mm; Conic constant = −2.273; N-BK-7 glass, source fiber-lens separation = 1.867 mm, receiving fiber-lens separa-tion = 2.146 mm, total track = 6.013 mm).

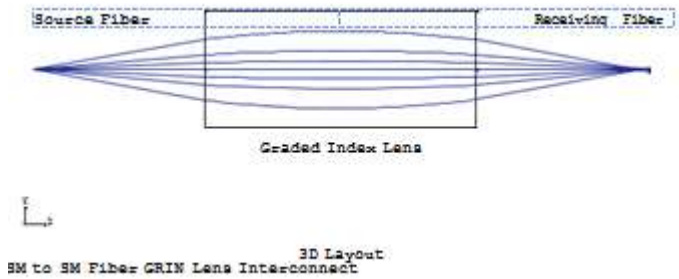

Fig. 3. Diagram showing the SMF-to-SMF coupling using uncoated GRIN rod lens (Lens diameter = 2.00 mm; Length = 4.00 mm, source fiber-lens separa-tion = 2.541 mm, receiving fiber-lens separation = 2.541 mm, total track = 9.082 mm).

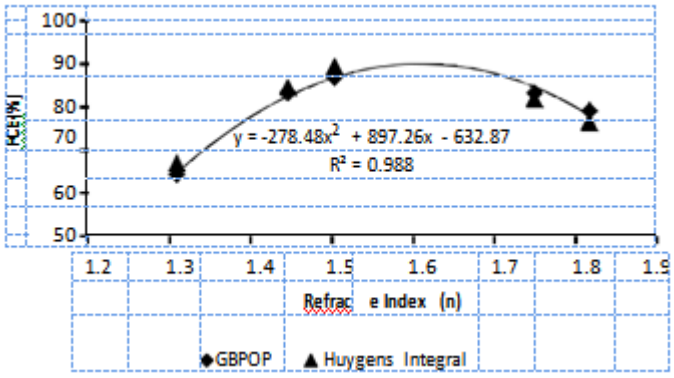

Fig. 4. Uncoated ball lens FCE calculations for sapphire (n = 1.74999), N-LASF9 glass (n = 1.81745), N-BK7 glass (n = 1.50358), S-LAH79 glass (n = 1.31) and fused silica (n = 1.44680) lenses at 1.310 m. The calculations were carried out using GBPOP and Huygens integral methods.

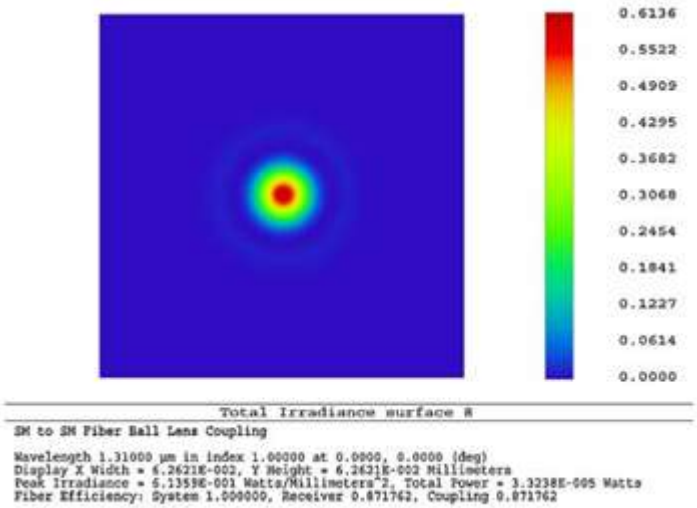

Fig. 5. Plot showing the calculated FCE of uncoated N-BK7 glass ball lens without accounting for Fresnel reflection and bulk absorption effects using GBPOP method in Zemax. The receiving and source fiber beam waists (x and y) were set to 4.6 m. The calculated FCE = 87.17% (x-sampling = y-sampling = 1024).

III. RESULTS AND DISCUSSION

In order to determine the ball lens material which can provide the highest FCE between two SMFs, FCEs were calculated for ball lenses made out of sapphire, N-LASF9 glass, N-BK-7 glass, S-LAH79 glass and fused silica using Huygens integral and GBPOP methods in Zemax at 1.310 m. As shown in Fig. 4, the highest FCE was achieved at 91.8% using the Huygens integral method for uncoated N-BK7 glass ball lens. Whereas, 87.17% FCE was achieved using the GBPOP for the same uncoated N-BK7 ball lens as depicted in Fig. 5. The worst FCE was calculated for uncoated N-LASF9 ball lens at 78.994%. The average difference between the Huygens integral and the GBPOP methods for all ball lens materials shown in Fig. 4 was 0.449%.

Additionally, the impact of misalignment on FCE was exam-ined by calculating the FCE for uncoated ball lens as a function of lens decentering (Fig. 6), lens tilts (Fig. 7), separation between the lens and the receiving fiber (Fig. 8), separation between the lens

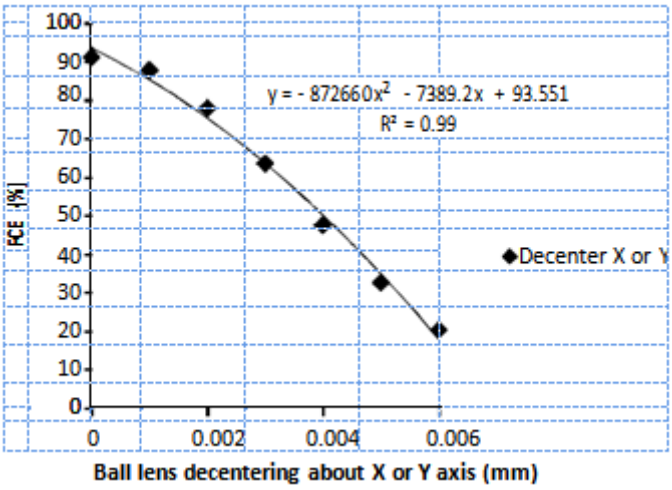

Fig. 6. Plot showing the relationship between FCE of uncoated N-BK7 glass ball lens and the lens decentering along the X-axis or Y-axis.

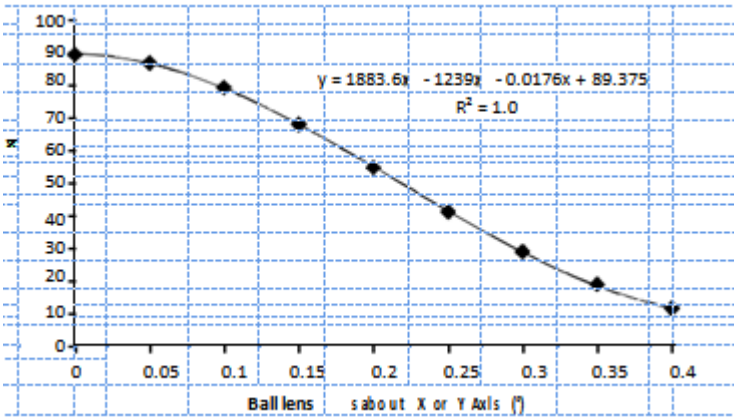

Fig. 7. Plot showing the relationship between FCE of uncoated N-BK7 glass ball lens and the lens tilts about the X-axis or the Y-axis.

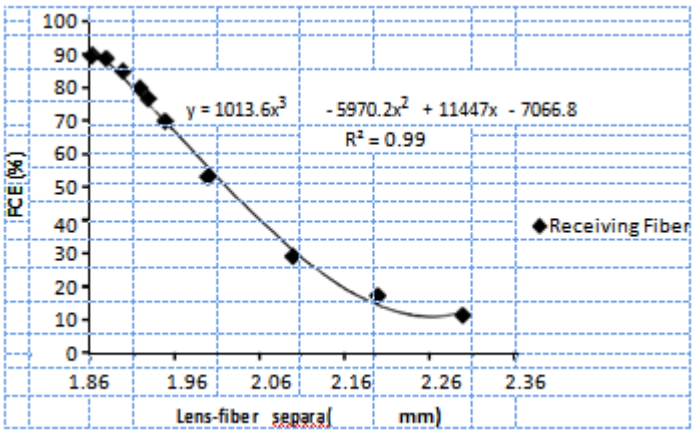

Fig. 8. Plot showing the relationship between FCE of uncoated N-BK7 glass ball lens and the lens to receiving fiber separation along the optical axis (start separa-tion = 1.863 mm).

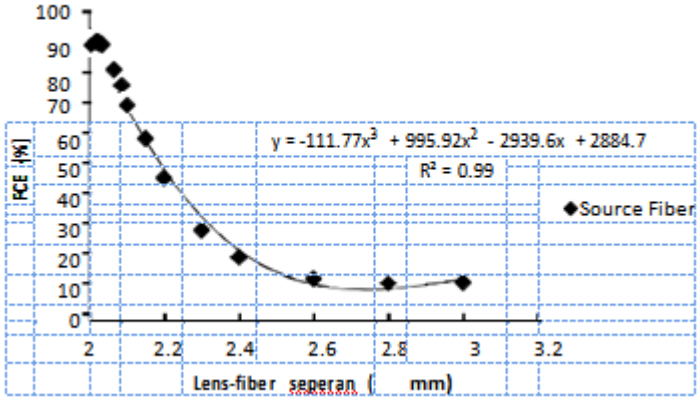

Fig. 9. Plot depicting the relationship between FCE of uncoated N-BK7 glass ball lens and the lens to source fiber separation along the optical axis (start separa-tion = 2.013 mm).

and the source fiber (Fig. 9), the source and receiving fiber decen-tering (Fig. 10), and the source and receiving fiber tilts (Fig. 11). Next, the linear portion of each graph was fitted into a straight line (Y = mx + c) employing linear regression (shown in each graph

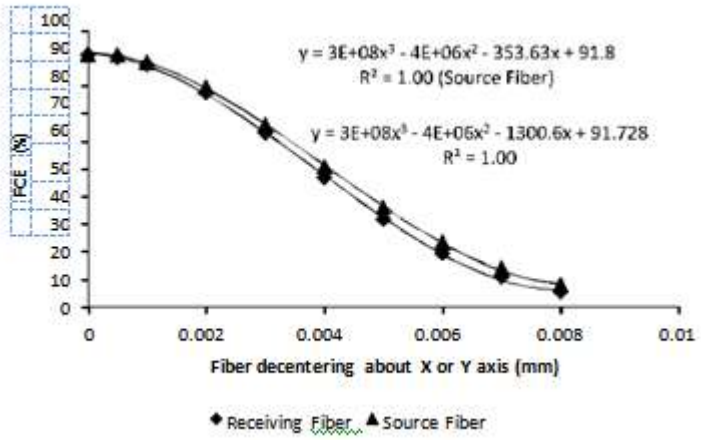

Fig. 10. Plot showing the relationship between FCE of uncoated N-BK7 glass ball lens and the source or receiving fiber decentering along the X-axis or Y-axis.

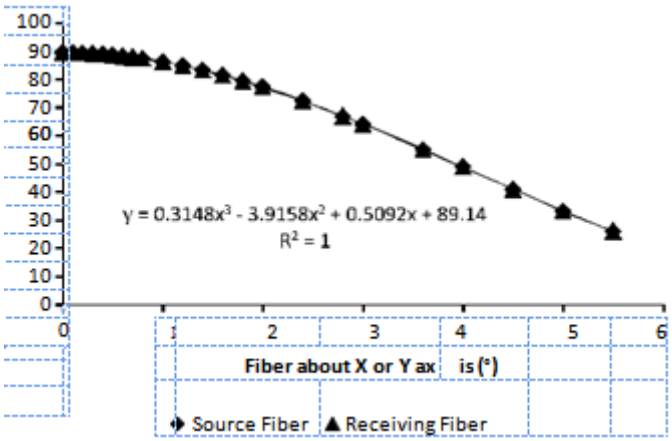

Fig. 11. Plot showing the relationship between FCE of uncoated N-BK7 glass ball lens and the source or receiving fiber tilts about the X-axis or Y-axis.

Table 1

Table summarizing the calculated slopes (% FCE per mm or degree) due to tilting and decentering the components of uncoated N-BK7 glass ball lens coupling scheme.

	FCE (mm) Dec. X	FCE (mm) Dec. Y	FCE (mm) Dec. Z	FCE (°) X-axis tilt	FCE (°) Y-axis tilt
Source fiber	±14,578	±1478	±179.1	±11.727	±11.727
Ball lens	±14,071	±14,071	–	±253.09	±253.09
Receiving fiber	±14,743	±14,743	±284.23	±11.727	±11.727

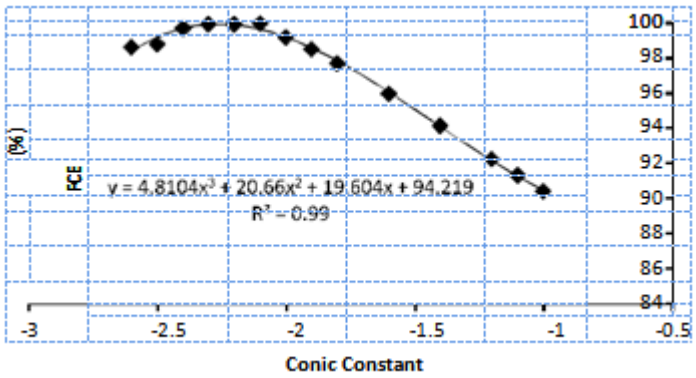

Fig. 12. Plot illustrating the relationship between the FCE of uncoated N-BK7 glass conic lens and the value of the lens conic constant.

as a solid line). Table 1 summarizes the slopes calculated for each straight line.

Likewise, the impact of misalignment on FCE was examined for uncoated conic lens coupling scheme. Fig. 12 depicts the relation-ship between FCE and the lens conic constant for uncoated N-NK-7 glass lens. As shown in Fig. 2 the maximum FCE is achieve at conic constant equal to −2.273. Figs. 13–17 depict the calculate curves for the FCE as a function of the conic lens decentering, lens tilts, lens-to-fiber separation, fiber decentering and fiber tilts, respectively. Table 2 summarizes the slopes calculated for the straight portion of the graphs shown in Figs. 13–17.

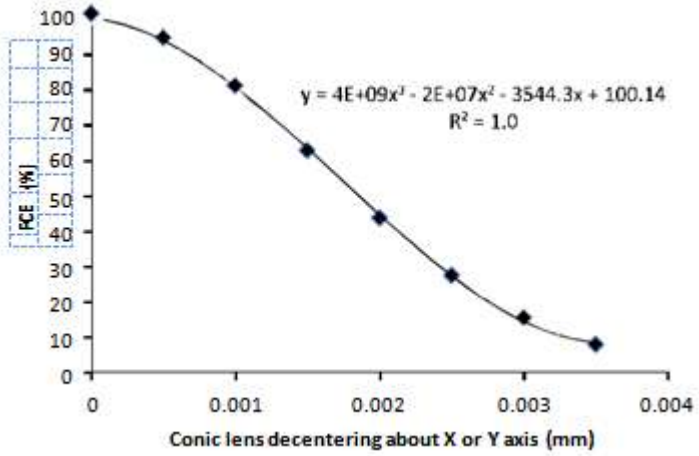

Fig. 13. Plot showing the relationship between FCE of uncoated N-BK7 glass conic lens and the decentering of the lens along the X-axis or Y-axis.

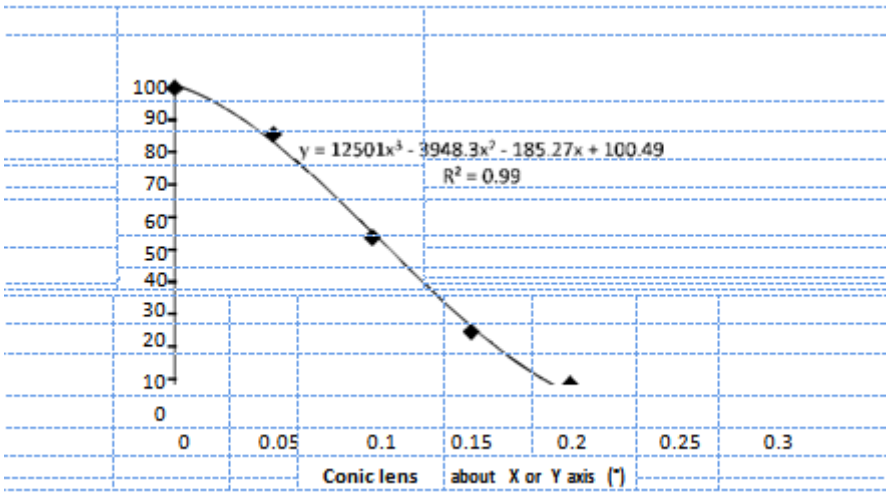

Fig**. 14.** Plot showing the relationship between FCE of uncoated N-BK7 glass conic lens and the lens tilts about the X or the Y-axis.

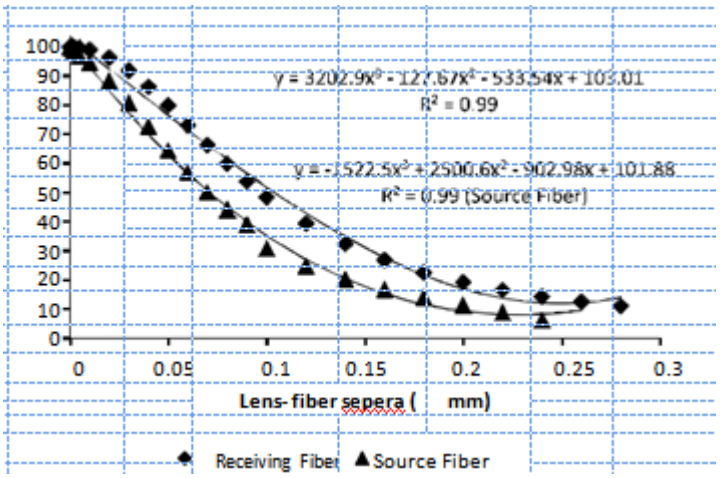

Fig. 15. Plot showing the relationship between FCE of uncoated N-BK7 glass conic lens and the receiving or the source fiber separation along the optical axis (source fiber to lens start separation = 1.888 mm; receiving fiber to lens start sepa- ration = 2.167 mm).

Based on the data tabulated in Tables 1–3 it can be seen that the

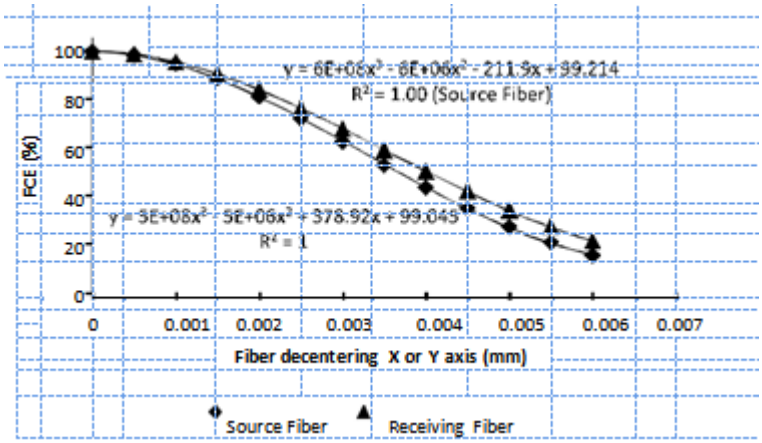

Fig. 16. Plot showing the relationship between uncoated N-BK7 glass conic lens FCE and the source or receiving fiber decentering along the X-axis or Y-axis.

Similarly, tolerance analysis was performed for the uncoated GRIN lens coupling scheme. Figs. 18–23 illustrate the obtained FCE curves for the GRIN lens scheme as a function of lens decentering, lens tilts, lens-to-fiber separation, fiber decentering and fiber tilts, respectively.

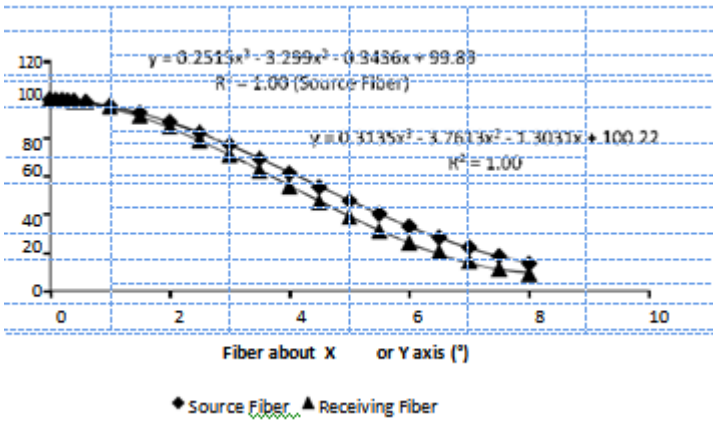

Fig. 17. Plot showing the relationship between the FCE of uncoated N-BK7 glass conic lens and the receiving and the source fiber tilts about the X-axis or Y-axis.

Table 2
Table summarizing the calculated slopes (% FCE per mm or degree) due tilting and decentering the components of the uncoated N-BK7 glass conic lens coupling scheme.

	FCE (mm) Dec. X	FCE (mm) Dec. Y	FCE (mm) Dec. Z	FCE (°) X-axis tilt	FCE (°) Y-axis tilt
Source fiber	±18,547	±18,547	±740.67	±14.03	±14.03
Conic lens	±33,332	±33,332	–	±522.14	±522.14
Receiving fiber	±16,946	±16,946	±606.23	±15.80	±15.80

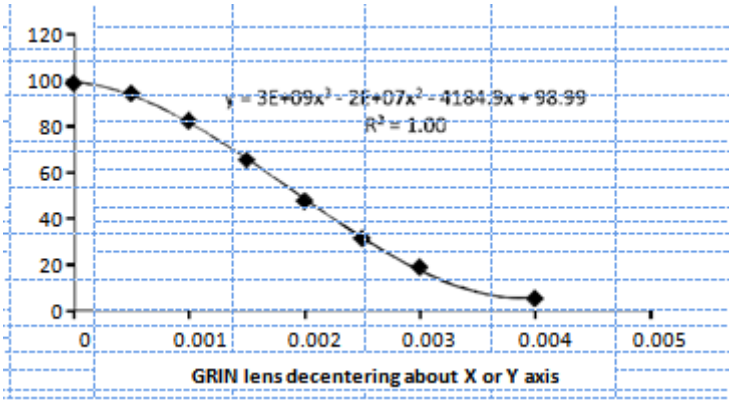

Fig. 18. Plot showing the relationship between the GRIN rod lens FCE and the decen- tering of the lens along the X-axis or Y-axis.

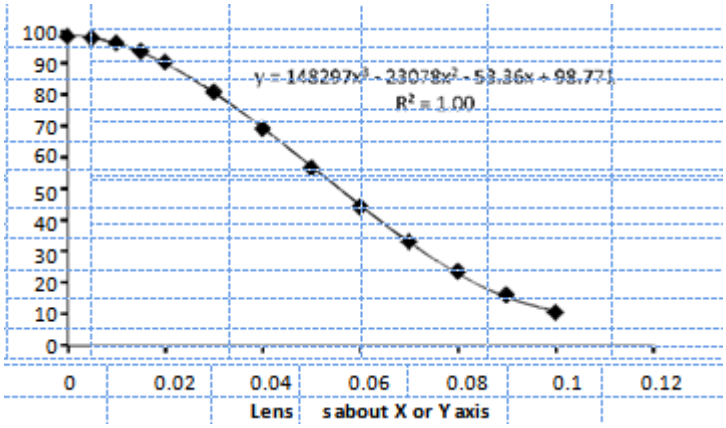

Fig. 19. Plot showing the relationship between FCE of uncoated GRIN rod lens and the lens tilts about the X-axis or the Y-axis.

GRIN lens coupling scheme is the most sensitivite coupling scheme for misalignment and the ball lens coupling scheme is the least sen-sitive coupling scheme for misalignment. Furthermore, the threelens coupling schemes are most sensitive to the lens decentering about the x and y-axis followed by the lens-to-fiber separation. Additionally, the calculations indicate that misalignment due to

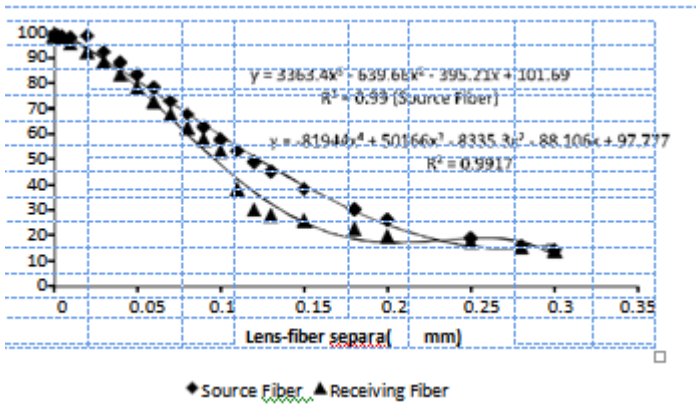

Fig. 20. Plot showing the relationship between the FCE of GRIN rod lens and the receiving and the source fiber separation along the optical axis (source fiber to lens start separation = 2.541 mm; receiving fiber to lens start separation = 2.541 mm).

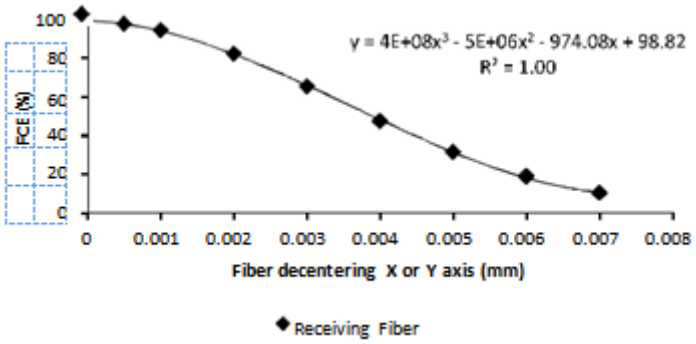

Fig. 21. Plot showing the relationship between FCE of uncoated GRIN rod lens and the receiving fiber decentering along the X-axis or Y-axis.

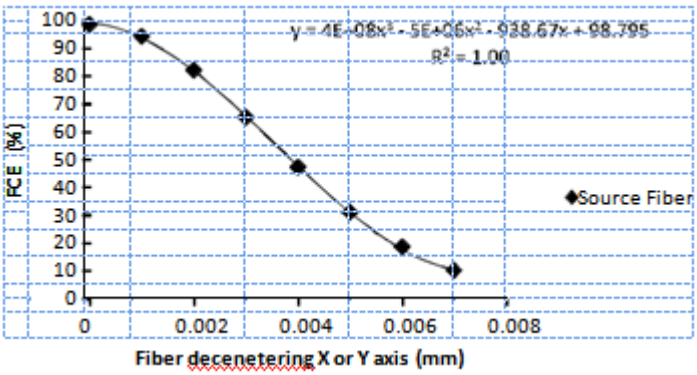

Fig. 22. Plot showing the relationship between uncoated FCE of GRIN rod lens and the receiving fiber decentering along the X-axis or Y-axis.

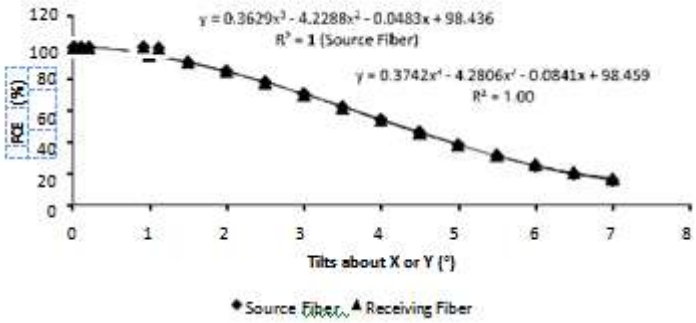

Fig. 23. Plot showing the relationship between FCE of uncoated GRIN rod lens and the receiving and the source fiber tilts about the X-axis or Y-axis.

Table 3 Table summarizing the calculated slopes (% FCE per mm or degree) due to tilting and decentering the components of uncoated single GRIN rod lens coupling scheme.

	FCE (mm) Dec. X	FCE (mm) Dec. Y	FCE (mm) Dec. Z	FCE (°) X-axis tilt	FCE (°) Y-axis tilt
Source fiber	±15,610	±15,610	±481.55	±15.69	±15.69
GRIN lens	±34,128	±34,128	–	±1102.9	±1102.9
Receiving fiber	±16,080	±16,080	±486.27	±15.79	±15.79

lens tilts has a higher impact on the FCE than the source or receiving fiber tilts.

IV. CONCLUSIONS

Based on the results reported in this article the following con-clusions can be drawn:

(1) The deviation between the Huygens integral and GBPOP SMF coupling efficiency calculations is <0.5%.
(2) The uncoated conic lens coupling scheme provides the highest coupling efficiency with coupling efficiency reaching 99.68% for N-BK7 glass lens followed by the uncoated GRIN lens coupling scheme at 96.58% FCE.
(3) Fresnel reflections and bulk absorption account for approxi-mately 7.76% of the FCE value and can be reduced to <3% using anti-reflection coatings.
(4) The ball lens coupling scheme has the shortest total track (pack-age length) equal to 5.875 mm and the GRIN lens has the longest total track equal to 9.082 mm.
(5) The GRIN lens SMF coupling scheme is the most sensitive scheme for misalignment and the ball lens coupling scheme is the least sensitive coupling scheme for misalignment.
(6) The FCE for the three lens coupling schemes is most sensitive to the decentering of the lens.

REFERENCES

[1] Jeff Hecht, Understanding Fiber Optics, third ed., Prentice Hall, Upper Saddle River, NJ, 1999.
[2] Ivan Landany, Laser to single-mode fiber coupling in the lab, Appl. Opt. 32 (June (18)) (1993) 3233–3236.
[3] Masud Mansuripur, Launching light into a fiber, Opt. Photon. News 12 (8) (2001) 56–59.
[4] Sami D. Alaruri, et al, System and Method Including Analytical Units, Patent Application WO2012012779 A2, July 22, 2011. https://www.google.com/patents/WO2012012779A2?cl=en&dq=sami+alaruri&hl=en&sa=X&ei=4CNcUtPBM8bLkQfp3oCYAQ&ved=0CDcQ6AEwAA .
[5] Sami D. Alaruri, et al., An endoscopic imaging system for turbine engine pres-sure sensitive paint measurements, Opt. Lasers Eng. 36 (3) (2001) 277–287.
[6] Sami D. Alaruri, et al., Development of a fiber optic probe for thermographic phosphor measurements in turbine engines, Opt. Lasers Eng. 22 (1) (1995) 17–31.
[7] Sami D. Alaruri, et al., Mapping the surface temperature of turbine engine components using laser induced fluorescence of thermographic phosphor, Opt. Lasers Eng. 31 (5) (1999) 345–351.
[8] D. Rogers, Ball lenses for coupling and collimation, Lightwave 16 (2) (1999) 104–109.
[9] Robert Gale Wilson, Ball-lens coupling efficiency for laser-diode to single-mode fiber: comparison of independent studies by distinct methods, Appl. Opt. 37 (May (15)) (1998) 3201–3204.
[10] Richard P. Ratowsky, Long Yang, Robert J. Deri, Kok Wai Chang, Jeffrey S. Kall-man, Gary Trott, Laser diode to single-mode fiber ball lens coupling efficiency: full-wave calculation and measurements, Appl. Opt. 30 (May (15)) (1997) 3435–3438.
[11] Holger Karstensen, Karsten Drogemuller, Loss analysis of laser diode to single-mode fiber couplers with glass spheres or silicon plano-convex lenses, J. Lightwave Technol. 8 (5) (1990) 739–747.
[12] Kyung S. Lee, Frank S. Barnes, Microlenses on the end of single-mode optical fibers for laser applications, Appl. Opt. 24 (Oct. (19)) (1985) 3134–3139.
[13] Christopher A. Edwards, Herman M. Presby, Corrado Dragone, Ideal microlenses for laser to fiber coupling, J. Lightwave Technol. 11 (2) (1993) 252–257.
[14] Robert Gilsdorf, Joseph C. Palais, Single-mode fiber coupling efficiency with graded-index rod lenses, Appl. Opt. 33 (June (16)) (1994) 3440–3445.
[15] W. Emkey, Jack Curtis, Analysis and evaluation of graded-index fiber-lenses, J. Lightwave Technol. LT-5 (9) (1987) 1156–1164.
[16] R.E. Wagner, W.J. Tomlinson, Coupling efficiency of optics in single-mode fiber components, Appl. Opt. 21 (Aug. (15)) (1982) 2671–2688.
[17] A. Nicia, Lens coupling in fiber-optic devices: efficiency limits, Appl. Opt. 20 (Sept. (18)) (1981) 3136–3145.
[18] Masatoyo Sumida, Kenji Takemoto, Lens coupling of laser diodes to single-mode fibers, J. Lightwave Technol. LT-2 (June (3)) (1984) 305–311.
[19] Carla Pitchlynn, Algorithm determines efficiency of fiber-coupling calculation, Laser Focus World (July) (2003) 63–65, PennWell Corporation, Tulsa, OK, USA.
[20] SUSS MicoOptics, Technical information sheet 07-Fiber Coupling, Issue 02-04 http://www.amstechnologies.com/fileadmin/amsmedia/downloads/ 2087 SMO TechInfo Sheet 07.pdf .

[21] Mark Nicholson, How to model coupling between single-mode fibers, radi-ant Zemax, Knowl. Base (2005), August 3, http://www.zemax.com/support/ knowledgebase/how-to-model-coupling-between-single-mode-fibers .
[22] Zemax LLC http://www.zemax.com release 13, Aug, 2014.
[23] Zemax LLC, Lens files: Ball coupling.SES/Conic interconnect.SES/ GRINinterconnect.SES. (example lens files provided with the Zemax lens design code).
[24] David T. Neilson, Tolerance of optical interconnections to misalignment, Appl. Opt. 38 (April (11)) (1999) 2282–2290.
[25] Corning, Inc., Corning SMF-28 CPC6 single-mode optical fiber, Product Infor-mation Data Sheet, publication no. PI1036, 1999.